Computational Fluid Dynamics JOURNAL vol.1 no.1 April 1992 (104 — 114)

NUMERICAL SOLUTION OF THREE DIMENSIONAL TURBULENT FLOW IN AN EQUILATERAL TRIANGULAR DUCT BY REYNOLDS STRESS MODEL

Hitoshi SUGIYAMA† Mitsunobu AKIYAMA† Masaru HIRATA‡
Satoshi UENO†

Abstract

A numerical calculation was carried out for the three dimensional flow in an equilateral triangular duct by using Reynolds stress model and a boundary fitted coordinate system. By Rodi's approximation, the Reynolds stress equations are transformed into the algebraic equations. The calculated result for the fully developed turbulent flow showed good agreement with experimental data measured in such flow and it clearly demonstrated the generation of a secondary flow of the second kind in developing turbulent flow, which is also experimentally observable.

1. INTRODUCTION

The flow in a duct with non-circular section is usually accompanied by a secondary flow, which is caused by the anisotropic character of the turbulence. This is called the secondary flow of the second kind. Although its strength is usually low, about only 2 to 5% of the bulk velocity, it shows considerable influence on the momentum and the heat transfer inside the duct. By transporting high momentum fluid towards the corners, it causes a bulging of the velocity and temperature contours towards the corners. This peculiarity of such flows has therefore motivated numerous research works. Extensive study on the square duct has been done both experimentally [1][2] and analytically [3][4]. Rectangular ducts have been examined by Tracy [5] and Leutheusser [6]. Although most of the non-circular ducts concerned are of square or rectangular sections, Aly, Trupp and Gerard [7] performed both experimental and analytical studies on the fully developed turbulent flow in a duct with an equilateral triangular section. However, these numerical analyses have been done on the assumption of the fully developed turbulent flows, and few works are available concerning to the entrance region. In the present paper, the experiment by Aly *et al.* was adopted and the turbulent flow in the entrance region was investigated, with emphasis on the development of the secondary flow of the second kind which is caused by the anisotropy of the turbulent flow. The adequacy of the adopted turbulence model was checked by comparing the numerical results with the experimental data. The numerical analysis used employed a boundary fitted coordinate system (hereafter designated as BFC), which facilitates establishment of the boundary conditions in enclosures with complicated shapes. The governing equations including the Reynolds stress equations were transformed from the physical plane into the calculation one in accordance with the BFC system.

Presented at the 4th Numerical Fluid Dynamics Symposium – Tokyp on December 20 – 22, 1990.
Received on January 30, 1991. Revised on July 24, 1991.

† Dept. Mech. Systems Engrg., Utsunomiya University; Utsunomiya 321 Japan
‡ Dept. Mech. Engrg., University of Tokyo; Tokyo 113 Japan

2. TECHNIQUE OF ANALYSIS

Nature of the anisotropy of the turbulence can be expressed by the Reynolds stress equations. Nevertheless, an analysis fully conserving the accuracy of these equations is not possible and some kinds of modeling was required. A set of the differential equations governing the transport of the Reynolds stresses is derived from the Navier-Stokes equation, namely:

$$\begin{aligned}\frac{\mathrm{D}\,\overline{u_iu_j}}{\mathrm{D}t} &= -\left[\overline{u_iu_k}\frac{\partial U_j}{\partial X_k}+\overline{u_ju_k}\frac{\partial U_i}{\partial X_k}\right]+\overline{\frac{p}{\rho}\left(\frac{\partial u_i}{\partial X_j}+\frac{\partial u_j}{\partial X_i}\right)} \\ &\quad -\frac{\partial}{\partial X_k}\left[\overline{u_iu_ju_k}-\nu\frac{\partial\,\overline{u_iu_j}}{\partial X_k}-\overline{\frac{p}{\rho}(\delta_{jk}u_i+\delta_{ik}u_j)}\right]-2\nu\overline{\frac{\partial u_i}{\partial x_k}\frac{\partial u_j}{\partial x_k}}\end{aligned} \tag{1}$$

The first term of the right hand is the production term P_{ij}, the second term is the pressure-strain correlation π_{ij}, the third term is the diffusion term Diff_{ij} and the fourth term is the dissipation term v_{ij}. For the convection and diffusion terms, the stress equations use the approximation proposed by Rodi [8], which performs the calculations by means of an algebraic stress model. By Rodi's approximation, these terms expressed in a differential form for Reynolds stress components can be transformed into the algebraic equation form as follows.

$$\begin{aligned}\frac{\mathrm{D}\,\overline{u_iu_j}}{\mathrm{D}t}-\mathrm{Diff}_{ij} &= \frac{\overline{u_iu_j}}{K}\left(\frac{\mathrm{D}K}{\mathrm{D}t}-\mathrm{Diff}_k\right) \\ &= \frac{\overline{u_iu_j}}{K}(P_k-v), \\ P_k &= -\overline{u_ku_\ell}\frac{\partial U_k}{\partial X_\ell}\end{aligned} \tag{2}$$

The pressure-strain correlation is a term which dose not appear in the turbulent energy equation. It dose not contribute to the balance of the total energy, but determines the redistribution of the energy in different components. Especially troublesome feature of the Reynolds stress equation is in what way we express the pressure-strain correlation term. Following Chou [9], the pressure-strain term can be expressed as follows:

$$\overline{\frac{p}{\rho}\frac{\partial u_i}{\partial X_j}}=\frac{1}{4\pi}\int_{\mathrm{VOL}}\left\{\overline{\left(\frac{\partial^2u_\ell u_m}{\partial x_\ell\partial x_m}\right)'\frac{\partial u_i}{\partial x_j}}+2\left(\frac{\partial U_\ell}{\partial X_m}\right)'\overline{\left(\frac{\partial u_m}{\partial X_\ell}\right)'\left(\frac{\partial u_i}{\partial X_j}\right)}\right\}\frac{d\,\mathrm{VOL}}{|\boldsymbol{x}-\boldsymbol{y}|}+S_{ij} \tag{3}$$

where the terms with and without a prime relate to values at $\boldsymbol{y}$ and $\boldsymbol{x}$, respectively. The first and second terms of the right hand side of (3) are relevant to the interaction of the fluctuating velocities and to that of the mean strain and the fluctuating velocities, respectively. The term S_{ij} represents the wall effect. We adopted the Rotta's linear return-to-isotropy model. Rotta's proposal for $\pi_{ij,1}$ may be written as

$$(\pi_{ij,1}+\pi_{ji,1})=-c_1\frac{v}{K}(\overline{u_iu_j}-\frac{2}{3}k) \tag{4}$$

where k and v are the time-averaged turbulence kinetic energy and the energy dissipation rate.

For $\pi_{ij,2}$ the correlation can be approximated in the form

$$\pi_{ij,2}=(\frac{\partial U_\ell}{\partial X_m})a_{ij}^{m\ell} \tag{5}$$

Table 1: Presure-strain correlation

$\pi_{ij,1}$	$-c_l \frac{v}{K}(\overline{u_i u_j} - \frac{2}{3}k\delta_{ij})$
$\pi_{ij,2} + \pi_{ji,2}$	$-\frac{c_2+8}{11}(P_{ij} - \frac{2}{3}P_k\delta_{ij}) + \zeta k(\frac{\partial U_i}{\partial X_j} + \frac{\partial U_j}{\partial X_i})$ $-\frac{8c_2-2}{11}(D_{ij} - \frac{2}{3}P_k\delta_{ij})$
$[\pi_{ij} + \pi_{ji}]_w$	$c_1 = c_1^* + c_1' f(\frac{L}{X_w}), \quad c_2 = c_2^* + c_2' f(\frac{L}{X_w}), \quad \zeta = \zeta^* + \zeta' f(\frac{L}{X_w})$

$$P_{ij} = -\overline{u_i u_k}\frac{\partial U_j}{\partial X_k} - \overline{u_j u_k}\frac{\partial U_i}{\partial X_k}, \qquad D_{ij} = -\overline{u_i u_k}\frac{\partial U_k}{\partial X_j} - \overline{u_j u_k}\frac{\partial U_k}{\partial X_i}$$

where

$$a_{\ell j}^{mi} = -\frac{1}{2\pi}\int_{\mathrm{VOL}} \frac{\partial^2 \overline{u_m' u_i}}{\partial \xi_\ell \partial \xi_j}\frac{d\,\mathrm{VOL}}{|\boldsymbol{x}-\boldsymbol{y}|} \tag{6}$$

and $a_{\ell j}^{mi}$ is the forth-order tensor. In this study, the forth-order tensor is determined by the following kinematic constraints.

$$a_{\ell ij}^{mi} = a_{\ell j}^{im} = a_{j\ell}^{im} \tag{7}$$

$$a_{\ell i}^{mi}\frac{\partial U_i}{\partial X_m} = 0 \tag{8}$$

$$a_{jj}^{mi} = 2\overline{u_m u_i} \tag{9}$$

These constraints presented by Gessner and Eppich [10] are different from Rotta's [11] proposal constraints in refer to the form of (8). We adopted the above constraints for the reason that $\pi_{ij,2}$ is defined as the product between the fourth order tensor and mean strain as shown in (5). The constraints in the form of (7) and (8) arise from symmetry and mass conservation, respectively. Moreover, as Rotta observed, the constraint form of (9) can be derived from Green's theorem. The form of (9) suggests that the forth-order tensor might be approximated by linear combination of Reynolds stresses. The most general such tensor satisfying the symmetry constraints implied by (7) may be written as

$$\begin{aligned} a_{\ell j}^{mi} \;=\; & \alpha\delta_{\ell j}\overline{u_m u_i} + \beta(\delta_{ml}\overline{u_i u_j} + \delta_{mj}\overline{u_i u_l} + \delta_{il}\overline{u_m u_j} + \delta_{ij}\overline{u_m u_\ell}) \\ & + c_2\delta_{mi}\overline{u_\ell u_j} + \{\eta\delta_{mi}\delta_{\ell j} + \nu(\delta_{m\ell}\delta_{ij} + \delta_{mj}\delta_{i\ell})\}k, \end{aligned} \tag{10}$$

which is indicated by Launder, Reece and Rodi [12]. The application of (8) and (9) enables two constants of (10) to be expressed in terms of C_2. On combining (5) and (10), the complete influence of the mean strain on the pressure-strain correlation may be expressed. The pressure-strain correlation terms and constants used in this model are shown in the Tables 1 and 2, respectively.

In handling these redistribution terms, the wall effect term $\pi_{ij,w}$ on turbulent stresses contains the function $f(L/X_w)$, as shown in the Table 1. It expresses the influence of the wall

Table 2: Constants in pressure-strain correlation

c_1^*	c_2^*	ζ^*	c_1'	c_2'	ζ'
1.4	0.44	−0.16	−0.35	0.12	−0.1

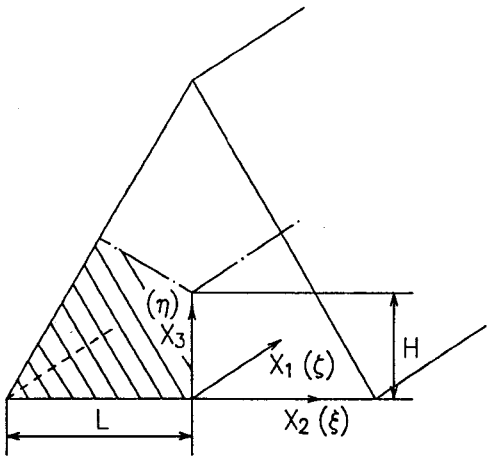

Fig.1:
Calculated region and the coordinate system

and takes the value 1 in its vicinity, approaching to 0 with the increasing distance of it. X_w expresses the horizontal distance from the wall, usually being defined by many different ways. Here was utilized the definition by Gibson and Launder [13] as follows:

$$f(\frac{L}{X_w}) = \frac{c_\mu^{3/4} k^{3/2}}{\kappa v} \frac{1}{X_w}, \qquad \frac{1}{X_w} = \frac{1}{X_1} + \frac{1}{X_2} + \frac{1}{X_3}. \tag{11}$$

The fourth term of (1) is the homogeneous part of dissipation. This term is modeled commonly with the assumption of the isotropic motion for the dissipation, namely:

$$v_{ij} = \frac{2}{3}\delta_{ij} v. \tag{12}$$

The calculation technique using BFC considers a coordinate system which fits to the boundaries of the real object to be analyzed. It then performs a coordinates transformation from the analysis domain of the physical space to the calculation domain, solving the physical phenomenon in the calculation space. The coordinates transformation into the calculation space is accomplished according to the following mathematical proposition:

$$\frac{\partial}{\partial X_i} = \frac{\partial \xi}{\partial X_i}\frac{\partial}{\partial \xi} + \frac{\partial \eta}{\partial X_i}\frac{\partial}{\partial \eta} + \frac{\partial \zeta}{\partial X_i}\frac{\partial}{\partial \zeta}. \tag{13}$$

Here, X_i stands for the coordinates system of the physical space (X_1, X_2, X_3) and ξ, η and ζ stand for the coordinates system of the calculation space.

3. ANALYSIS RESULTS AND CONSIDERATIONS

The object of the analysis is the entrance region of an equilateral triangular duct as shown in

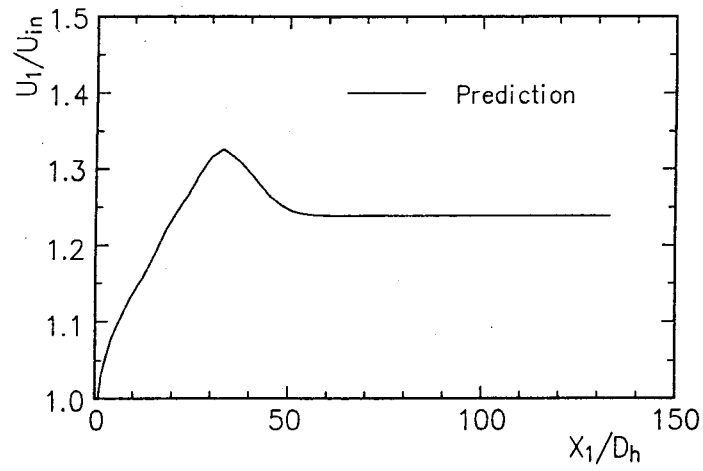

Fig.2:
Axial velocity variation along the centerline

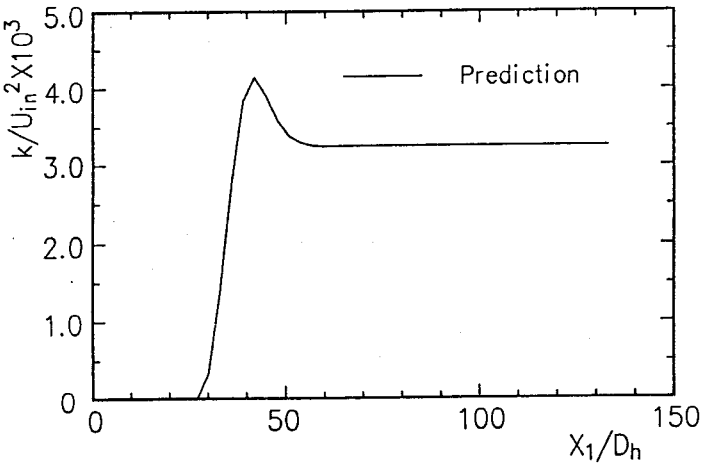

Fig.3:
Axial turbulent energy variation along the centerline

Fig.1. Taking into account the symmetric nature of its cross section, the calculation object can be divided into three equal parts of irregular quadrilateral shapes, the calculation being performed over only one of them. To enable comparisons between the numerical computations and the experimental facility used by Aly, Trupp and Gerard, the Reynolds number was set to 53,000, and the calculation domain was defined as the entrance region of 133 D_h in the direction of the main flow, and D_h stands for the hydraulic diameter. Considering that Demuren and Rodi [14] analyzed the turbulent flow in a duct of square section at a distance of 84 D_h, the entrance region of 133 D_h is expected to represent a fully developed flow condition. The parameters of the mesh utilized in this calculations were set to $(\xi \times \eta \times \zeta) = (15 \times 15 \times 50)$, with a special refinement in the vicinity of the walls. The number of grids 15x15 for calculating section were determined to take into account the calculated results reported by Gosman and Rapley [15]. They have reported that the solution are substantially independent for grid numbers of about 250 and greater for half section of triangular duct. A condition of isotropic turbulent flow with constant velocities was adopted at the inlet. The turbulent energy k and the turbulence dissipation v are unknown to the experimental data, so that the values of $k = U_b \times 10^{-5}$,

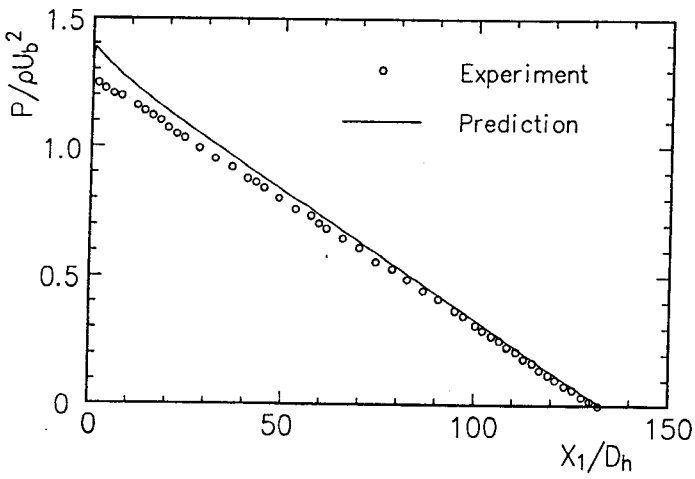

Fig.4:
Static pressure distribution along the duct axis

$v = k^{3/2}/D_h$ were adopted at the inlet section. The Neumann conditions were adopted at the outlet section. Concerning boundary condition of k and v, the consistence of the universal velocity distribution at the vicinity of the wall and also the supposition of local equilibrium lead to the utilization of the law of the wall function. Before the calculation is carried out for the triangular duct, we applied the present model the developing flow in a square duct, which is experimented by Melling and Whitelaw [2], in order to examine the validity of the model. As a result of this calculation, it was clear that the present method was able to predict characteristic phenomenon for the developing flow in a square duct [16].

Figure 2 shows the development of the main flow velocity in the central core region U_1, which is normalized by the inlet velocity U_{in}. Noticeable in this calculated results is a local peaking of the developing turbulent flow in the entrance region. This occurs when the developing velocity boundary layer originated at the wall surfaces reaches the central portion. The momentum is then exchanged by mutual interferences, and the velocity come to a peak value there. This takes place at a distance of $33\,D_h$ from the inlet, which is similar to the results by Demuren and Rodi for the turbulent flow in a square duct.

Figure 3 outlines the development of the turbulent energy along the duct centerline. Similarly to the main flow velocity, there is a peak value at $42\,D_h$, which locates slightly downstream than the one of the velocity peak. Both of the main flow velocity and the turbulent energy, after passing their local peaks, decrease and gradually approach constant values.

Figure 4 shows the axial pressure distribution along the duct centerline, where ρ and U_b represent the density and the bulk velocity, respectively. This values tend to coincide with the experimental ones far downstream, although they are higher in the region near the inlet. The friction factor is given as follows:

$$f = \frac{D_h\left(-\frac{\partial P}{\partial X_1}\right)}{\rho U_b^2/2}. \tag{14}$$

The friction factor asymptotes to $f = 2.016 \times 10^{-2}$, which is higher than the value of $f = 1.965 \times 10^{-2}$ observed in the experiments. On the other hand, the calculated value is by 3 %

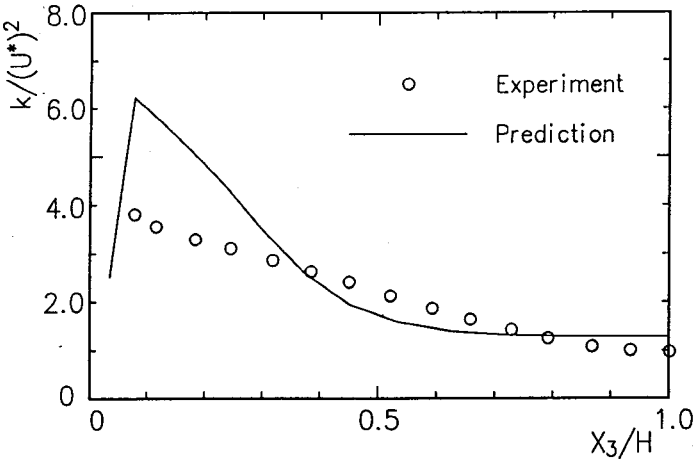

Fig.5:
Turbulent energy along the mid-wall bisector

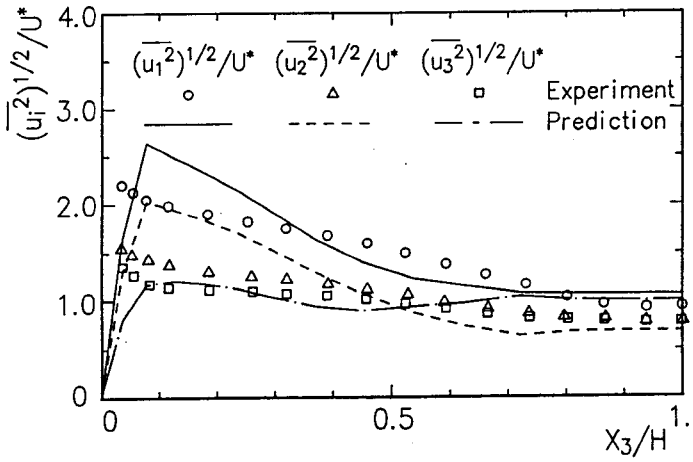

Fig.6:
Normal stresses along the mid-wall bisector

lower than the value of $f = 2.083 \times 10^{-2}$ obtained by the empirical formula of Blausius. It seems that the friction factor of a triangular duct is smaller than that of a smooth circular tube.

Figures 5 to 8 describe the calculated results at $X_1 = 133\,D_h$, which is located in the fully developed region. All the quantities are made dimensionless by the average frictional velocity U^*. Figures 5 and 6 shows the distributions of the turbulent energy and the normal stresses at the mid wall bisector, respectively. The turbulent energy shows a remarkable increase close to the wall as seen in Fig.5, which due to the stronger velocity gradients as shown in Fig.8 (a) which compares the predicted velocity contours to the experimental results. Because the production term of the turbulent energy is affected by the derivative of the mean velocity. On the other hand, observing the central portion, it can be noticed that the turbulent energy decreases rapidly and gradually approaches to the experimental values.

The normal stresses distributions along X_3 direction are shown in Fig.6. The turbulence model utilized here enables us to confirm the strong anisotropy in the vicinity of the walls.

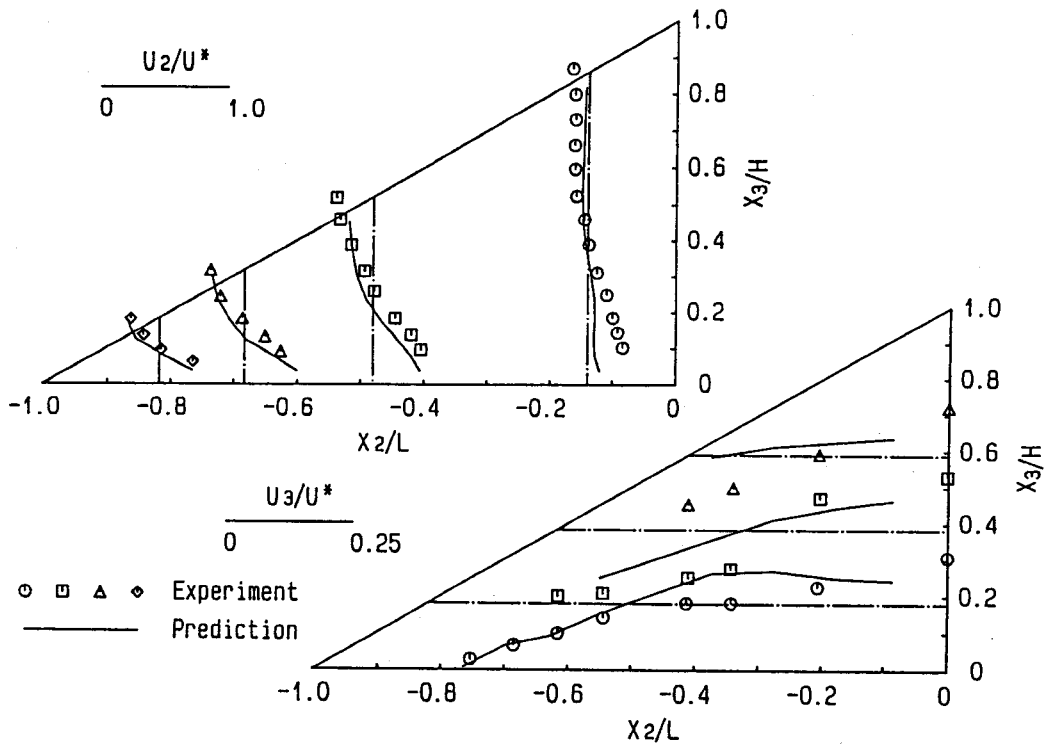

Fig.7: Distributions of the secondary velocity U_2 and U_3

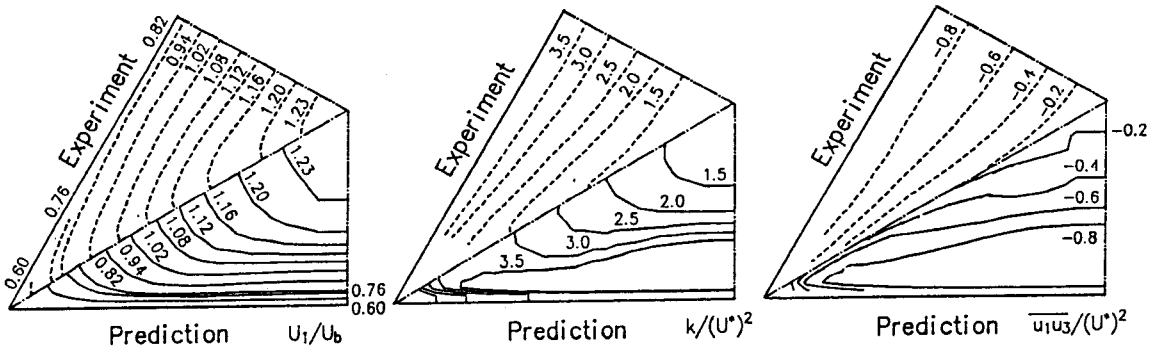

(a) mean velocity (b)turbulent energy (c) shear stress u_1u_3

Fig.8: Comparison of the calculated results with the experiment

This aspect changes if one moves towards the center region, where isotropic flow redistribute gradually the energy between the normal stresses. Figures 7(a) and (b) show the velocity distribution of U_2 and U_3, which express the magnitude of the secondary flow of the second kind. According to the distribution of U_2, the velocity is expected to become low in the mid-wall region, but it is strongly controlled by the coefficients C_1 and C_2 of the pressure strain terms. The present model has a tendency to underestimate the values of the secondary flow of the second kind. Figures 8(a), (b) and (c) compare the main flow velocity distribution, the turbulent energy and the shear stresses with the experimental values, respectively. One can observe, in general, good agreement between them, but there are also noticeable disagreements in the neighborhood of the wall surfaces. The turbulence energy contours calculated show stronger distortion toward the corner than the mean flow velocity along the symmetry line has. The experimental contours also exhibit such tendency. The secondary flow vector, the mean flow velocity contours and the contours of the turbulent energy along the mean flow direction are illustrated in Fig.9, at three different positions of $X_1 = 10.0\,D_h$, $42.0\,D_h$ and $130.2\,D_h$ from the inlet of triangular duct. At the first stage, one pair of vortices of secondary flows of the second kind appears in the corner region as seen at $X_1 = 10.0\,D_h$. As the flow develops, the centers of the vortices move gradually towards the central region, reaches the position closest to the center at about $X_1 = 42.0\,D_h$ and then turns towards the corner again. The mean velocity contours distort closer to the corner as a result of momentum transfer by the secondary flow along the bisector. The distortion of the mean velocity contours is observed larger at $X_1 = 42.0\,D_h$ than at other two positions. It can also be noticed that the secondary flow reaches its maximum value at approximately $X = 33.1\,D_h$, then decreases and is stabilized. This may suggest that the maximum value of the secondary flow of the second kind appears near the region where the local peaking of the axial center-line velocity is generated as a result of shear layer interaction. A high region of the turbulent energy exists near the corner at $X_1 = 10.0\,D_h$ and extends its area along the wall as the mean flow develops. At $X_1 = 10.0\,D_h$, the location of the high turbulent energy coincides with the generation point of the secondary flow. These phenomena imply that the secondary flow is not firstly generated along the corner bisector, but occurs along the vicinity of wall. The secondary flow along the corner bisector may be derived as result of the generation of the flow along the wall to satisfy mass conservation.

4. CONCLUSIONS

A numerical analysis has been made on three-dimensional developing turbulent flow in a triangular duct using a modified Reynolds stress equation model and a boundary fitted coordinate system. We especially improved the pressure strain correlations of the Reynolds stress equation. As a result of comparison with the experimental data, the validity of this modified model has been confirmed. The present model has been able to predict characteristic phenomena of fully developed flow but has estimated the level of the secondary flow of the second kind smaller than the experimental value. Moreover, we analyzed the development of the secondary flow of the second kind in developing flow. It was made clear that the maximum value of the secondary flow is observed near the region where local peaking of the axial center-line velocity is generated as a result of shear layer interaction.

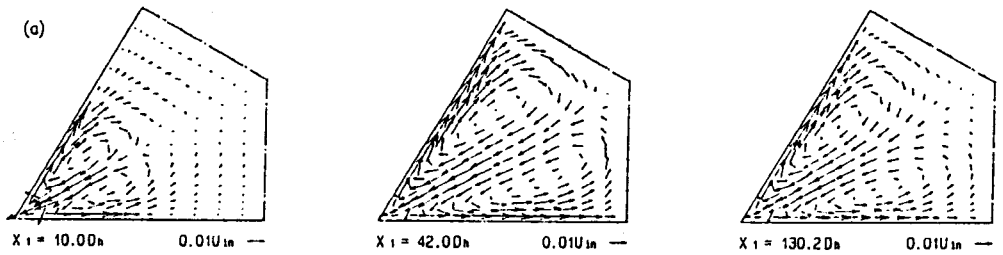

(a): secondary flow of the second kind

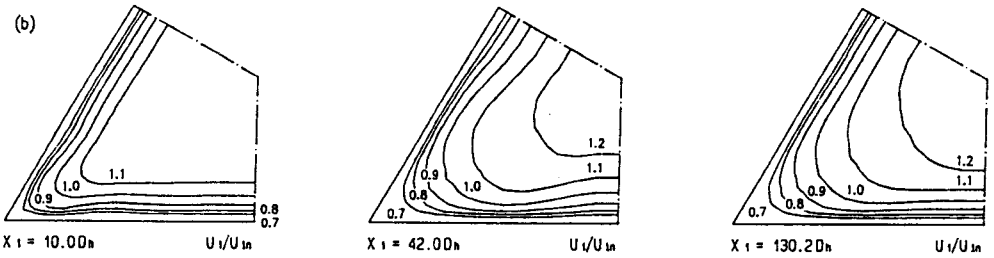

(b): mean velocity

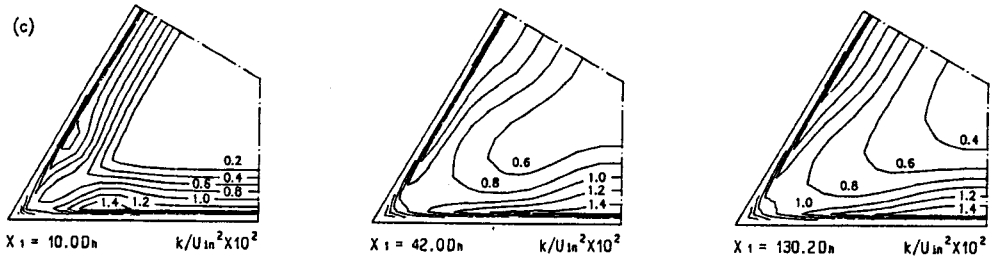

(c): turbulent energy

Fig.9: Predicted contours in developing turbulent flow

REFERENCES

[1] E.Brundrett and W.D.Baines (1964) The production and diffusion of vorticity in duct flow; J. Fluid Mech., vol.19 pp.375-394

[2] A.Melling and J.H.Whitelaw (1976) Turbulent flow in rectangular duct; J. Fluid Mech., vol.78 pp.289-315

[3] B.E.Launder and W.M.Ying (1973) Prediction of flow and heat transfer in ducts of square cross-section; Heat and Fluid Flow, Vol.3 pp.115-121

[4] F.B.Gessner and A.F.Emery (1976) A Reynolds stress model for turbulent corner flows: Part 1 Development of the model; J. Fluid Engineering, vol.98 pp.261-268

[5] H.J.Tracy (1965) Turbulent flow in a three-dimensional channel; J. Hydral. Div. A.S.C.E. vol.91(HY6) pp.9-35

[6] H.J.Leutheusser (1963) Turbulent flow in rectangular ducts; J. Hydral. Div. A.S.C.E. vol.89(HY3) pp.1-19

[7] A.M.M.Aly, A.C.Trupp and A.D.Gerrard (1978) Measurements and prediction of fully developed turbulent flow in an equilateral triangular duct; J. Fluid Mech., vol.85 pp.57-83

[8] W.Rodi (1976) A new algebraic relation for calculating the Reynolds stresses; Z. Angew. Math. Mech., vol.56 pp.T219-T221

[9] P.Y.Chou (1945) On velocity correlations and the solutions of the equations of turbulent fluctuation; Quart. Appl. Math. vol.3 pp.38-54

[10] F.B.Gessner and H.M.Eppich (1981) A near wall pressure-strain model for turbulent corner flows; Proc. 3rd. Symp. Turbulent Shear Flows, Davis, pp.2.25-2.32

[11] J.Rotta (1951) Statistische theorie nichthomogener turbulenz; Zeitschrift für Physik., Bd.129 pp.547-572

[12] B.E.Launder, G.J.Reece and W.Rodi (1975) Progress in the development of a Reynolds stress turbulence closure; J. Fluid Mech., vol.68 pp.537-566

[13] M.M.Gibson and B.E.Launder (1978) Ground effects on pressure fluctuations in the atmospheric boundary layer; J. Fluid Mech., vol.86 pp.491-511

[14] A.G.Demuren and W.Rodi (1984) Calculation of turbulence-driven secondary motion in non-circular ducts; J. Fluid Mech., vol.140 pp.189-222

[15] A.D.Gosman and C.W.Rapley (1978) A prediction method for fully-developed flow through non-circular passages; Proc. Int. Conf. Numerical Meth. Paper FS 178, pp.271-285

[16] H.Sugiyama, M.Akiyama and T.Serizawa (1991) Numerical analysis of developing flow in a square duct using Reynolds stress model; Proc. ASME/JSME Thermal Engineering Joint Conf., pp.159-165